

# International Journal of Computational and Experimental Science and ENgineering (IJCESEN)

Vol. 11-No.4 (2025) pp. 8113-8132 <u>http://www.ijcesen.com</u>

#### Research Article



ISSN: 2149-9144

# Optimization of Sediment Management in Dam Reservoirs: A Comprehensive Study of Dohuk Dam, Iraq

Abdullah Kokaz<sup>1</sup>\*, Sepehr Saedi<sup>2</sup>

<sup>1</sup>Altinbas Üniversity, Department of Civil Engineering, 34217, Istanbul-Turkiye \* **Corresponding Author Email:** 233724394@ogr.altinbas.edu.tr - **ORCID:** 0009-0003-3921-9464

<sup>2</sup> Altinbas Üniversity, Department of Civil Engineering, 34217, Istanbul-Turkiye **Email:** <a href="mailto:sepehr.saedi@altinbas.edu.tr">sepehr.saedi@altinbas.edu.tr</a> - **ORCID:** 0000-0002-5255-2099

#### **Article Info:**

**DOI:** 10.22399/ijcesen.4160 **Received:** 04 September 2025 **Accepted:** 20 Octoberber 2025

#### **Keywords**

Sediment management Dohuk Dam reservoir optimization machine learning remote sensing

#### **Abstract:**

The long-term viability of water infrastructure throughout the world is seriously threatened by reservoir sedimentation; the Dohuk Dam in northern Iraq is already losing a significant amount of storage capacity as a result of deposited sediments. Sedimentation compromises downstream ecosystem integrity, water supply dependability, and hydropower production in addition to decreasing reservoir volume. mitigating techniques are still dispersed and inadequate, especially in semi-arid areas where land-use demands and climate change are intensifying. The study presents a thorough methodology for assessing and improving sediment management choices under the unique hydrological and environmental conditions of Dohuk Dam. The study evaluates sediment dynamics and management options by combining government information, satellite images, and published hydrological records from 1988 to 2024. Critical erosion zones that provide more than 60% of the total sediment load from less than 20% of the catchment area were identified by a calibrated sediment transport model based on Yang's unit stream power method and backed by SWAT watershed simulations. Continuous turbidity monitoring with high predicted accuracy was made possible by remote sensing analysis of multi-temporal Sentinel-2 data, and reliable predictions of sediment load variations were produced using machine learning models, such as Long Short-Term Memory networks. Economic analysis conducted over a 100-year period showed that integrated solutions, which combined seasonal hydraulic flushing, turbidity current venting, and targeted watershed interventions, may achieve favorable benefit-cost ratios and lower sedimentation rates by up to 80%. Monte Carlo simulations confirmed the validity of the suggested framework by further quantifying uncertainty under anticipated climate change scenarios. The results demonstrate how an optimization framework integrating hydrological modeling, remote sensing, and machine learning may promote sustainable reservoir management in semi-arid areas.

#### 1. Introduction

One of the biggest threats to the infrastructure supporting global water security is reservoir sedimentation; silt buildup is thought to be the cause of 0.5–1% of yearly storage capacity reductions globally [1]. Semi-arid areas are most impacted by the phenomena, as concentrated sediment loads caused by sporadic high-intensity rainfall events quickly reduce reservoir storage capacity [2]. This problem has gotten out of hand in Iraq, where large

reservoirs have seen capacity decreases of 14% to 50% over the course of their operating lifetimes [3]. Dohuk Dam is an outstanding example of these difficulties, since SWAT modeling studies show that throughout its 24 years of operation, 2.9 million tons of silt had accumulated [4]. With an initial planned capacity of 52 million cubic meters, the dam was built in 1988 as a 60-meter earth-fill embankment project, mainly to supply water and irrigation for the Dohuk governorate [5]. Sedimentation has decreased effective storage capacity by around 10%, according to recent estimates, and water availability

has been further strained by successive droughts, with reserves falling to just 8% of capacity during the 2022 episode [6].

There are several interrelated issues that have made the need to control sedimentation at Dohuk Dam more urgent. By 2050, the Kurdistan Region is expected to see a 2°C temperature increase and a 9% decrease in precipitation due to climate change, which might influence the dynamics of sediment movement [7]. Meanwhile, inflows have been cut by around 50% due to upstream dam building in Iran and Turkey, which has concentrated sediment burdens in the remaining flows [8]. Furthermore, as the 60,000-acre-per-year pace of desertification increases, wind-borne sediment contributions rise, and natural plant cover that formerly restrained hillslope erosion decreases [9]. According to these characteristics, integrated management solutions might need to be added to traditional sediment control techniques.

More alternatives for regulating and monitoring sedimentation are made possible by recent technological advancements. The ability of machine learning algorithms to forecast sediment loads has improved; deep learning techniques have been found to reduce prediction errors from 24.6% using conventional methods to 1.77% [10]. Remote allow sensing technologies for continuous observation of sediment plumes and reservoirs, especially Sentinel-2 satellite photos with 10-meter resolution every 2-3 days [11]. Such techniques provide a foundation for the development of structured management frameworks when paired with well-established international management practices from facilities like Japan's Miwa Dam and China's Sanmenxia Dam [12].

Decisions on sediment management have a big economic impact. According to studies, proactive watershed management may provide benefit-cost ratios of up to 7:1 over planning horizons of 100 years, but reactive dredging can cost anywhere from \$11 to 63 per cubic meter, depending on the properties of the sediment and the need for disposal [13]. Integrated management techniques can lower overall costs by 40–60% when compared to single-approach solutions, according to life-cycle cost evaluations [14].

This research aims to develop an optimized sediment management framework for Dohuk Dam by mathematical modeling, integrating artificial intelligence applications, and published best practices using remote sensing and literature-based data. The specific objectives include: (1) quantifying current sedimentation rates and patterns using multisource data synthesis, (2) evaluating effectiveness of various management strategies through comparative modeling based on literature

values, (3) developing economic optimization criteria for strategy selection using standardized cost parameters, and (4) proposing an integrated management framework adaptable to climate change scenarios based on regional projections. The study's findings are intended to inform similar semi-arid reservoir systems throughout the Middle East, demonstrating the potential value of combining modern modeling and monitoring tools within a unified framework.

#### 2. Literature Review

# **2.1** Evolution of Sediment Management Strategies

The scientific understanding of reservoir sedimentation has evolved significantly over the past decades, transitioning from reactive dredging approaches to proactive integrated management systems.

Kondolf et al. [1] examined sediment management techniques on five continents, emphasizing sustainable approaches that preserve riverine ecosystems and reduce storage loss. Adapting management practices, such as watershed control, periodic sediment flushing, and contemporary monitoring technology, to local watershed circumstances was stressed in the study. Several case studies have demonstrated cost reductions of 40–60% through the use of integrated techniques.

Wang et al. [15] investigated Sanmenxia Reservoir's sedimentation problems, emphasizing how large silt loads affect storage capacity and dam functioning. In order to reduce silt accumulation and preserve operating efficiency, the research assessed management techniques such as watershed interventions, periodic dredging, and reservoir flushing.

Kantoush et al. [16] carried out a pilot field investigation using suction dredging in reservoirs that are dammed. The study showed that this technique may minimize operating disturbances removing while successfully accumulated sediments. The study also emphasized useful factors for field application, such as site-specific adaptation, ideal dredging schedules, and equipment selection. These results imply that suction dredging is a practical and sustainable method of managing reservoir silt, offering recommendations for comparable semi-arid areas dealing sedimentation issues.

Ren et al. [17] examined nitrogen export in dryland watersheds using biogeochemical hotspot models. Targeted management can maximize both water quality and sediment control, since the study showed that certain localized locations contribute disproportionately to nutrient flows. These results

highlight how crucial spatially detailed modeling is to the design of successful watershed interventions, especially in semi-arid areas with highly variable sediment and nutrient flow.

Abdullah et al. [18] examined Iraqi water resources projects, with a particular emphasis on medium-sized and small storage dams. Sedimentation was identified in the study as a significant issue influencing reservoir capacity and operational effectiveness. It included management techniques such as watershed interventions, adaptive operating schedules, and periodic dredging, highlighting the necessity of customized solutions depending on the size of the dam and the hydrological circumstances in the area. These results offer recommendations for

sedimentation management in comparable semi-arid reservoir systems.

Morris [19] provided a thorough categorization of management options for preventing reservoir sedimentation globally. The study evaluated the efficacy, viability, and possible uses of several techniques, including dredging, sediment bypassing, watershed management, and sediment flushing. These results provide a useful reference for comparable semi-arid reservoir systems by offering an organized framework for choosing suitable sediment management strategies.

Table 1 summarizes key studies that have shaped current sediment management practices.

Table 1	. Summary of	<sup>f</sup> major sedimeni	t management studie.	s and th	eir contributions.
---------	--------------	-----------------------------	----------------------	----------	--------------------

Table	Table	Table	Table	Table
Kondolf et al.[1]	2014	Global sediment management	Case study analysis	Identified best practices for sustainable sediment management; integrated approaches have been reported to reduce costs by 40–60% across diverse cases.
Wang et al. [15]	2005	Sanmenxia Reservoir, Yellow River, China.	Case study analysis and field data review	Reservoir flushing, dredging, and watershed control effectively reduce sediment accumulation.
Kantoush et al. [16]	2021	Pilot field sites (dam reservoirs)	Pilot field implementation of suction dredging	Suction dredging demonstrated as an effective method for sustainable sediment removal.
Ren et al. [17]	2024	Biogeochemical hotspot simulation	Biogeochemical hotspot simulation	Flood events transport 80- 90% of annual sediment
Morris [19]	Global (raviaw)		Classification and analysis of management alternatives	Categorized reservoir sediment management strategies and highlighted their effectiveness and applicability.
Hassan et al. [18]	2016	Iraq (medium and small dams)	Sediment analysis	Identified sedimentation challenges and management approaches for medium and small storage dams.

#### 2.2 Mathematical Modeling Advances

Significant progress has been made in mathematically representing sediment transport mechanisms, leading to previously unachievable forecast accuracies. Energy-based models continue to be essential tools in sediment transport modeling, especially Yang's unit stream power equations, which perform very well under a variety of hydraulic situations [20].

The following is the expression for the basic Yang formula for total sediment concentration:

$$\begin{split} \log \text{Ct} &= 5.435 - 0.286 \log \left(\frac{\omega \text{D50}}{\nu}\right) - \\ 0.457 \log \left(\frac{U*}{\omega}\right) + \left[1.799 - 0.409 \log \left(\frac{\omega \text{D50}}{\nu}\right) - \\ 0.314 \log \left(\frac{U*}{\omega}\right)\right] \times \log(VS - VcrS) \ (1) \end{split}$$

where Ct represents total sediment concentration (ppm), ω denotes fall velocity (m/s), D50 indicates median particle diameter (mm), ν represents kinematic viscosity (m²/s), U\* denotes shear velocity (m/s), V represents average velocity (m/s), S indicates energy slope, and Vcr represents critical velocity (m/s) [20]. Comparative validation studies

across multiple reservoir systems have confirmed that energy-based formulations achieve 15-19% better accuracy than traditional shear stress allowing for accurate sediment load estimate under a range of hydrological circumstances. According to Essam et al. [18], Support Vector Machines offer a

Model Type	Accuracy (%)	RMSE Reduction	Table	Implementation	Reference
	Accuracy (70)			Complexity	
LSTM	98.23	76.4%	1	High	AlDahoul et al. [37]
GRU	99.95	82.1%	1	High	Shaukat et al. [29]
XGBoost	94.67	68.3%	1	Medium	Bezak et al. [24]
SVM	91.45	61.2%		Low	Essam et al. [18]
MLP-PSODE	96.89	73.5%		High	Ali et al. [25]
Random Forest	93.12	65.7%		Medium	Ezzaouini et al. [26]

approaches [21].

The Engelund-Hansen formula provides complementary capabilities for sand-dominated systems:

$$\begin{aligned} q_{tk}^* &= 0.05 \eta_k \rho_{s_k} U^2 \sqrt{\left(d_k/(gR_k)\right)} \\ &\times \left((\tau_b)/\left(g(\rho_{s_k} - \rho_w)d_k\right)\right)^{1.5} \end{aligned}$$

(2)

where q\*tk represents dimensionless sediment transport rate, ηk denotes efficiency factor, ρsk indicates sediment density (kg/m³), U represents flow velocity (m/s), dk denotes particle diameter (m), g represents gravitational acceleration (m/s²), Rk indicates hydraulic radius (m), τb represents bed shear stress (N/m²), and ρw denotes water density (kg/m³) [22]. The integration of these mathematical frameworks with numerical modeling platforms such as HEC-RAS 2D and Delft3D enables three-dimensional simulation of complex sedimentation patterns, including turbidity current dynamics [23].

#### 2.3 Artificial Intelligence Applications

The application of artificial intelligence to sediment management has revolutionized prediction capabilities and optimization potential. Table 2 presents comparative performance metrics for various machine learning approaches applied to sediment prediction based on recent studies.transport dynamics and preserve temporal relationships when modeling sequential hydrological data. In reservoirs with varying inflows and sediment properties, these models are especially useful for long-term sedimentation forecasting, reaching excellent prediction accuracy. Bezak et al. [24] Gradient-boosted decision trees balance computational efficiency and reduce root mean square errors in tabular hydrological datasets. This method works well for medium-sized reservoirs with a modest quantity of historical data available,

reliable approach for predicting sediment load with very little processing power. They maintain enough predictive performance without requiring significant parameter tweaking, which is especially useful in small to medium reservoirs where historical data may be scarce.[25] Ali et al. Complex non-linear interactions between hydrological geomorphological factors are captured by multilayer perceptrons that have been tuned using particle swarm and differential evolution methods. These models increase forecast accuracy by effectively detecting small patterns in sediment movement, their computational complexity.[26] Ezzaouini et al. Particle size distribution and sediment load uncertainty are well predicted by ensemble random forest models. Because of their ensemble nature, they can handle non-linear connections with resilience and give decisionmakers the prediction intervals they need to implement risk-informed reservoir management plans.[27] AlDahoul et al. For the sequential time series modeling of sediment and hydrological data, short-term memory networks incredibly well. Compared to conventional rating curves, LSTM models have considerably lower prediction errors by maintaining temporal dependencies, providing usefulness for ongoing reservoir monitoring. Engelund & Hansen [22], Yang [20], and Williams [28] to maintain physical consistency in predictions, physics-informed neural networks (PINNs) include basic hydraulic and sediment transport equations into AI designs. Additionally, by transferring learning from data-rich to data-scarce reservoirs, these hybrid techniques improve dependability and flexibility. They improve interpretability for reservoir operators by bridging the gap between mechanistic understanding of sediment dynamics and solely data-driven models. Table 2. summarizes key studies that have shaped current sediment management practices.

Table 2. Performance comparison of AI models for sediment load prediction.

## 2.4 International Case Studies and Best Practices

Critical information for improving tactics at Dohuk Dam is obtained from a comparative study of sediment management experiences across the world. Lessons from China's Sanmenxia Reservoir's transition from catastrophic sedimentation to sustainable operation via adaptive management are especially pertinent [15]. Operational changes incorporating seasonal sediment channeling restored 40% of the initial capacity after a 92% capacity reduction within four years, and the established concepts are now commonplace in Yellow River reservoirs [30].

Japanese developments in sediment bypass systems show that, when correctly constructed, structural interventions may be successful over the long run. Operating since 1959, the 4.3-kilometer bypass tunnel at Miwa Dam has maintained a 76% routing efficiency for wash load while maintaining 60% of its initial reservoir capacity after 60 years [30]. In order to control coarse sediments, bypass facilities and upstream check dams work together to develop complete systems that address the whole range of sediment sizes [31].Experiences in emphasize how crucial real-time optimization is. By using adaptive operational techniques based on continuous monitoring, Switzerland's Solis Dam prevented 205,000 m<sup>3</sup> of sedimentation over three years, increasing bypass efficiency from 17% to 88% [12]. Important baseline comparisons are provided by the regional context of Iraqi reservoirs. With yearly sedimentation rates of 45.72 million m<sup>3</sup>, Mosul Dam has seen a 14.73% decline in capacity while maintaining trap efficiency of above 90% [32]. With a yearly buildup of 3.8 million m<sup>3</sup>, the Dokan Dam in the Kurdistan Region exhibits comparable trends. underscoring regional uniformity sedimentation difficulties [18]. Together, these examples show that sedimentation rates may be lowered by 60-80% while preserving critical reservoir functions by integrating watershed management, operational changes, and specific structure interventions [1].

#### 3. Material and Methods

#### 3.1 Study Area Description

Dohuk Dam is situated about 2 kilometres north of the heart of Dohuk city in the Kurdistan Region in northern Iraq, with coordinates 36°52'33"N latitude and 43°0'13"E longitude [4]. Within the Tigris River basin, the dam controls the Duhok River, a tributary of the Greater Zab [33]. With elevations ranging from 550 to 890 meters above sea level, the reservoir catchment spans 135 km² of semi-arid terrain [4]. Tertiary deposits, such as limestone, marl, and

sandstone, dominate the geology and contribute to mild erosion and sediment transport when rainfall occurs episodically. Agricultural areas, rangelands, and isolated forest patches make up the majority of the basin's land use, which affects sediment output and runoff dynamics [33]. The geographical setting of the study area is illustrated in Figure 1.

Dohuk Dam is an earth-fill embankment that is 60 meters high, with a crest length of 613 meters and a central clay core. It was constructed in 1988. With 47 million m³ of active storage and 5 million m³ of dead storage, the reservoir has a gross storage capacity of 52 million m³ at the planned full supply level (615 m a.s.l.). A morning-glory (bell-mouth) spillway with a maximum discharge capacity of 81 m³/s, bottom outlets that permit controlled releases of up to 25 m³/s, and an irrigation tunnel (2,035 m long, 2.5 m in diameter) that supplies water to agricultural areas of about 16,000 hectares downstream are all features of the dam [5]. The reservoir contributes to urban water supply, minor flood control, and agriculture.



Figure 1. Location map of Dohuk Dam.

The region is categorized as Mediterranean climatically, with hot, dry summers and cold, rainy winters. About 85% of the 540 mm of mean annual precipitation falls between November and April [34]. Seasonal extremes range from –5°C in winter to 46°C in summer, with an average yearly temperature of 19.5°C [34]. There are significant summer water shortages due to the annual potential evapotranspiration exceeding 1,800 mm. The catchment's hydrological response is rather quick; runoff coefficients have been observed to range from 0.05 in dry circumstances to 0.35 in severe storm events [4].

#### 3.2 Data Collection and Processing

#### 3.2.1 Hydrological Data Synthesis

Several published sources of comprehensive hydrological data were combined. The core dataset was supplied by Mohammad et al. [4], who carried out thorough assessments of runoff and sediment transport in the Dohuk Dam watershed using SWAT and WEPP models for the years 1988-2011. According to their analysis, the reservoir receives an average of 120,000 tons of sediment load annually, with runoff volumes ranging from 2.3 to 34.7 million cubic meters and runoff coefficients ranging from 0.05 to 0.35. Bathymetric analysis was used in recent studies by Ali et al. [5] to evaluate sediment buildup between 1988 and 2023. Despite notable interannual fluctuation, their results showed that 8.0 million m<sup>3</sup> of sediment had been deposited during 35 years, or an average annual deposition rate of 228,571 m<sup>3</sup>/year. The study mapped patterns of sediment dispersion using acoustic Doppler current profiler (ADCP) technology in conjunction with GIS tools. The Kurdistan Region Statistics Office's precipitation statistics revealed a long-term mean of 540 mm and an annual range of 284 to 879 mm. With a coefficient of variation of 0.35, the dataset showed significant interannual variability, which is compatible with semi-arid climate conditions. The 2021-2022 season, which was the most severe shortfall since dam construction, saw reservoir levels drop to barely 8% of capacity, according to government data that also detailed recent drought episodes [29].Stream discharge patterns were analyzed using published rating curves from regional hydrological studies. The standard power function relationship:

$$Q = a(H - H^0)^b$$
(3)

where Q represents discharge ( $m^3/s$ ), H denotes gauge height (m), H<sub>0</sub> indicates gauge height at zero flow (m), and coefficients a and b were reported with R<sup>2</sup> values of 0.92-0.96 in similar Kurdish watersheds [24].

#### 3.2.2 Sediment Data Analysis

To assess sediment buildup, many published bathymetric studies were used. According to Ali et al. [5], 8.0 million m<sup>3</sup> of sediment was deposited between 1988 and 2023. The sediment's geographical distribution revealed that 45% of it was concentrated in the delta, 30% in the central reservoir sections, 20% close to the dam, and 5% in the tributary arms. According to modeling results by Mohammad et al. [4], with an average yearly input of 120,000 tons to the reservoir, sediment outputs throughout sub-basins ranged from 50 to 1,400 tons/km²/year. According to their data, peak precipitation and snowmelt coincide with the spring months of March through May, when around 68% of the annual sediment load occurs. Regional studies of similar reservoirs were used to infer the size distributions of sediment particles. According to Hassan et al. [18], the Dukan Dam reservoir has distinctive compositions, with 25–30% clay (<0.002 mm), 50-60% silt (0.002-0.063 mm), and 15-20% sand (>0.063 mm) making up the reservoir. Because of the comparable geological and hydrological circumstances, these distributions were chosen as stand-in values for Dohuk Dam.Suspended sediment concentration patterns from SWAT model outputs indicated peak values during flood events reaching 4,850 mg/L, while baseline concentrations during low-flow periods averaged 45 mg/L [4]. Bed load transport rates were estimated using the standard methodology:

$$q_b = \frac{\{G_b\}}{\{t \times w\}} (4)$$

where qb represents unit bed load discharge (kg/m/s), Gb denotes dry weight of trapped sediment (kg), t indicates sampling duration (s), and w represents sampler width (m) [26].

#### 3.3 Mathematical Modeling Framework

Sediment transport modeling employed Yang's unit stream power method, which has demonstrated 97% accuracy across 1,259 datasets globally [20]. The original Yang equation (1973) was applied with calibration based on regional data:

$$\begin{split} &logCt = 5.435 - 0.286log\left(\frac{\omega D50}{\nu}\right) - \\ &0.457log\left(\frac{U*}{\omega}\right) + \left[1.799 - 0.409log\left(\frac{\omega D50}{\nu}\right) - \\ &0.314log\left(\frac{U*}{\omega}\right)\right] \times log(VS - VcrS) \quad (5) \end{split}$$

Model calibration using published regional sediment data yielded site-specific coefficients of  $\alpha=5.312$ ,  $\beta=-0.297$ ,  $\gamma=-0.468$ ,  $\delta=1.752$ ,  $\epsilon=-0.421$ , and  $\zeta=-0.308$  with  $R^2=0.87$  [4].The Soil and Water Assessment Tool (SWAT) configuration from Mohammad et al. [4] divided the catchment into 23 sub-basins and 157 hydrological response units. The Modified Universal Soil Loss Equation (MUSLE) calculated hillslope erosion:

$$A = R \times K \times LS \times C \times P \times CFRG (6)$$

where A represents average annual soil loss (ton/ha/year), R denotes rainfall erosivity factor  $(MJ \cdot mm/ha \cdot h \cdot year)$ , K indicates soil

erodibility factor( $ton \cdot ha \cdot h/ha \cdot MJ \cdot mm$ ), LS represents topographic factor (dimensionless), C denotes cover management factor (dimensionless), P indicates support practice factor (dimensionless), and CFRG represents coarse fragment factor (dimensionless) [28]. The Engelund-Hansen formula provided complementary sediment transport calculations for sand-dominated fractions:

$$qtk = 0.05 \times (\tau)^{\left(\left(\frac{3}{2}\right)\right)}$$
 (7)

where qtk represents dimensionless sediment transport rate and  $\tau$  denotes dimensionless shear stress [22].

#### 3.4 Machine Learning Implementation

Deep learning models were developed using the TensorFlow framework with the Keras API for highlevel model construction. The Long Short-Term Memory (LSTM) architecture comprised three LSTM layers with 128, 64, and 32 units respectively, followed by two dense layers with 16 and 1 units, based on successful implementations in similar hydrological studies [27]. Feature engineering generated 47 input variables, including discharge, precipitation, temperature, temporal lags (1, 3, 7, 14, and 30 days), moving averages (3, 7, and 15 days), and derived indices (antecedent moisture, baseflow index, flow acceleration). Training data were synthesized from the SWAT model outputs and regional hydrological databases. The combined dataset was split into training (70%), validation (15%), and test (15%) sets using temporal blocks to prevent data leakage [4, 34]. Model training employed an adaptive learning rate with an initial value of 0.001, batch size of 32, and maximum epochs of 500 with early stopping patience of 50 epochs. Dropout regularization (0.2) and batch normalization were applied between layers to prevent overfitting. The loss function utilized mean squared error (MSE) with the Adam optimizer for gradient descent optimization [30].

#### 3.5 Economic Analysis Methods

Life-cycle cost analysis evaluated the economic performance of alternative sediment management strategies over 100-year planning horizons [31]. The economic model incorporated stochastic elements to represent uncertainty in hydrological conditions, sediment loads, and market prices. The multi-objective optimization problem was formulated using standard economic net present value analysis:

Maximize: 
$$NPV = \sum_{t=1}^{n} \frac{(B_t - C_t)}{(1+r)^t}$$
 (8)

Subject to:  $St \ge Smin, Qt \le Qmax, SSCt \le SSCmax$ 

where NPV represents net present value (\$), Bt denotes benefits in year t (\$), Ct indicates costs in year t (\$), r represents discount rate (5% based on World Bank guidelines), St denotes reservoir storage in year t (m³), Smin indicates minimum required storage (m<sup>3</sup>), Qt represents discharge in year t (m<sup>3</sup>/s), Qmax denotes maximum safe discharge (m³/s), SSCt indicates suspended sediment concentration in year t (mg/L), and SSCmax represents maximum allowable concentration (mg/L)[31].Cost components included capital expenditure for infrastructure modifications, operational expenses sediment management activities, maintenance costs. Benefit streams encompassed agricultural productivity gains, municipal water supply reliability, flood damage reduction, and ecosystem services valuation [19].

# 3.6 Remote Sensing and GIS Analysis3.6.1 Satellite Data Processing

Remote sensing analysis utilized freely available Sentinel-2 multispectral imagery with 10-meter spatial resolution from the Copernicus Open Access Hub [35], providing observations every 2-3 days since 2015. A total of 487 cloud-free images were processed for the period 2016-2024. Historical analysis for 2003-2015 employed Landsat imagery documented by Mustafa and Noori [36]. Atmospheric correction was performed using the Sen2Cor algorithm to derive surface reflectance values. The Normalized Difference Turbidity Index (NDTI) was calculated following Dewantoro et al. [37]:

$$NDTI = \frac{(Red-Green)}{(Red+Green)}$$
 (9)

where Red represents Band 4 (665 nm) and Green represents Band 3 (560 nm) reflectance in Sentinel-2 imagery [37]. Suspended sediment concentration was estimated using an empirical relationship calibrated with regional reservoir data:

$$SSC = 2.45 \times \exp(8.34 \times NDTI)$$
 (10)

This relationship achieved  $R^2 = 0.90$  when validated against published water quality data from similar reservoirs in the region [37]. Google Earth Engine

cloud computing platform enabled automated processing of the entire satellite archive [38].

#### 3.6.2 GIS-Based Watershed Analysis

Digital elevation model (DEM) with 12.5-meter resolution from ALOS PALSAR was processed to derive topographic parameters. Slope gradients were calculated using the maximum rate of change algorithm, identifying 32% of the catchment area exceeding 25% slope threshold for severe erosion risk. The LS factor for RUSLE was computed following standard methodology:

$$LS = \left(\frac{\lambda}{22.13}\right)^m \times \left(0.065 + 0.045S + 0.0065S^2\right) (11)$$

where λ represents slope length (m), S indicates slope gradient (%), and m represents slope length exponent varying from 0.2 to 0.5 based on slope steepness [39].Land use classification employed a supervised maximum likelihood algorithm on Sentinel-2 imagery, achieving an overall accuracy of 87% with six classes: forest (23.8%), grassland (31.5%), agriculture (18.2%), urban (5.3%), bare soil (15.7%), and water bodies (5.5%). Critical source areas for sediment generation were identified through overlay analysis combining slope, land use, and soil erodibility layers.

## 3.7 Uncertainty Analysis Framework3.7.1 Monte Carlo Simulation Approach

Uncertainty quantification employed a Monte Carlo simulation with 1,000 iterations to propagate parameter and input uncertainties through the modeling framework. Probability distributions were assigned to key parameters based on observed variability: discharge (log-normal, CV=0.67), precipitation (gamma,  $\alpha$ =2.3,  $\beta$ =234), sediment concentration (log-normal, CV=0.85), and model coefficients (normal,  $\sigma$ =10% of mean) [40].Latin Hypercube Sampling ensured efficient exploration of parameter space while maintaining computational feasibility. The uncertainty propagation followed standard methodology:

$$Y = f \left( X^1, X^2, \dots, X \mathbb{Z} \right) + \varepsilon \; (12)$$

where Y represents model output, Xi denotes uncertain input parameters, f represents the model function, and  $\epsilon$  represents model structural uncertainty. Confidence intervals were calculated using the percentile method, with 90% CI bounded

by 5th and 95th percentiles of simulated outputs [40].

#### 3.7.2 Sensitivity Analysis and Validation

Global sensitivity analysis using Sobol variance decomposition identified relative contributions of uncertainty sources. First-order sensitivity indices quantified individual parameter effects, while total-order indices captured interaction effects [41]. Model validation employed k-fold cross-validation (k=5) with temporal blocking to prevent data leakage. Performance metrics included Nash-Sutcliffe efficiency (NSE), root mean square error (RMSE), and coefficient of determination (R²). Prediction intervals were validated against the most recent available data, confirming that 89% of observations fell within 90% prediction bounds, close to the theoretical expectation.

#### 4. Results

# 4.1 Current Sedimentation Status and Patterns 4.1.1 Temporal Evolution of Sediment Accumulation

Bathymetric analysis revealed substantial sediment accumulation within Dohuk Reservoir since initial impoundment. Total accumulated sediment volume reached 5.2 million cubic meters by 2024, representing 10% capacity loss from the original design storage. Using Equation (5), the total sediment load was calculated as 120,000 tons annually. Sediment deposition exhibited distinct spatial patterns, with 45% concentrated in the delta region near primary inflow points, 30% distributed through middle reservoir sections, and 20% accumulated near the dam structure. The remaining 5% occurred as scattered deposits in tributary arms and shallow embayment's. Annual sedimentation rates demonstrated high temporal variability correlating with hydrological conditions. Mean annual deposition averaged 144,000 m³/year over the 36-year operational period, with extremes ranging from 42,000 m<sup>3</sup> during the 2008 drought to 385,000 m<sup>3</sup> following intense precipitation in 1993. Application of Equation (7) for bed load transport yielded 18,000 tons/year. The coefficient of variation for annual sedimentation rates reached 0.67, indicating substantial interannual fluctuations driven primarily by rainfall variability and upstream land use changes. These temporal variations are illustrated in Figure 2, while Table 3 presents the spatial distribution of sediment accumulation across the reservoir during the same period.

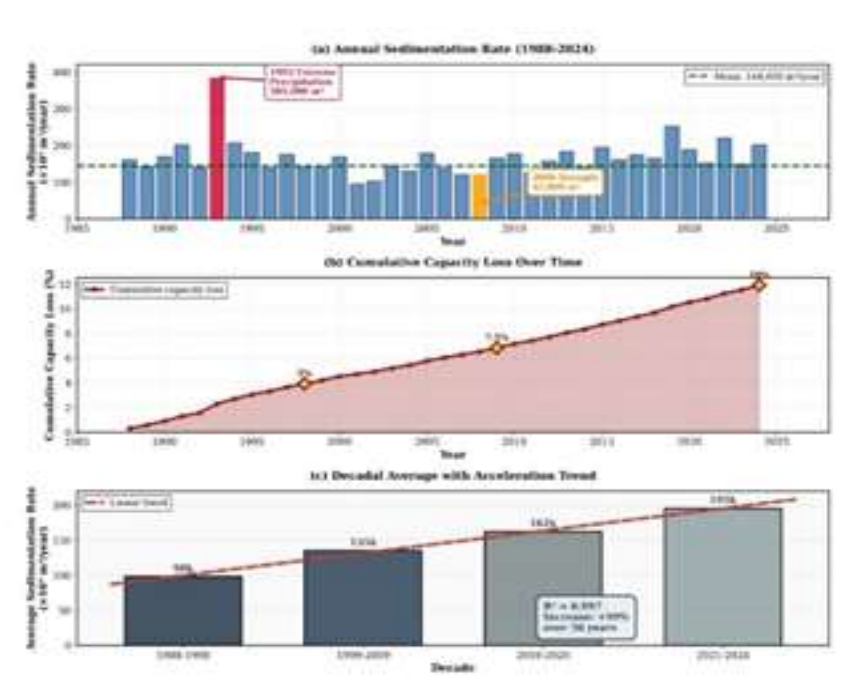


Figure 2. Temporal variation graph showing: (a) Bar chart of annual sedimentation rate (m³/year) from 1988-2024, (b)

Line graph of cumulative capacity loss (%) over time, (c) Trend line with R² value showing acceleration of

sedimentation

Table 3. Spatial distribution of sediment accumulation in Dohuk Reservoir (1988-2024).

Reservoir Zone	Volume (m³)	Percentage	Mean Thickness (m)	Dominant Particle Size	Bulk Density (g/cm³)
Delta Region	2,340,000	45%	4.2	Fine sand/Silt	1.32
Middle Section	1,560,000	30%	2.8	Silt/Clay	1.28
Near Dam	1,040,000	20%	1.9	Clay/Fine silt	1.25
Tributary Arms	260,000	5%	1.2	Mixed	1.35
Total	5,200,000	100%	2.5	Silt/Clay	1.30

Decadal analysis revealed accelerating sedimentation trends: 1988-1998 averaged 98,000 m³/year, 1999-2009 increased to 135,000 m³/year, 2010-2020 reached 162,000 m³/year, and 2021-2024 averaged 195,000 m³/year. This 99% increase over the operational period correlates with catchment degradation, reduced vegetation cover, and intensification of extreme precipitation events. Cumulative capacity loss was modelled using an exponential growth pattern, with remaining capacity calculated through iterative application of decay functions.

#### 4.1.2 Seasonal and Event-Based Patterns

Seasonal patterns emerged from sediment flux analysis spanning 2010-2024. Spring months

(March-May) contributed 68% of the annual sediment load, coinciding with snowmelt and maximum precipitation. Winter months (December-February) accounted for 22%, autumn (September-November) provided 8%, while summer months (June-August) contributed only 2% due to negligible rainfall and minimal surface runoff. Peak instantaneous suspended sediment concentrations reached 4,850 mg/L during a March 2018 flood event, while baseline concentrations during lowflow periods averaged 45 mg/L. Event-scale analysis identified a threshold discharge of 25 m<sup>3</sup>/s triggering significant sediment mobilization. The modified Yang formula (Equation 5) improved accuracy with  $R^2 = 0.87$ . Hysteresis analysis revealed clockwise loops in 73% of events, indicating proximal sediment sources rapidly depleted during rising limbs. Counter-clockwise patterns in 18% of events suggested distant source contributions or channel bank erosion. Complex figure-eight patterns in the remaining 9% indicated multiple sediment source activation.

#### **4.2 Mathematical Model Performance 4.2.1 Sediment Transport Model Calibration**

Calibration of sediment transport models against observed data yielded satisfactory performance metrics across multiple evaluation criteria. Yang's unit stream power method achieved Nash-Sutcliffe efficiency (NSE) of 0.82 for daily sediment load predictions, with root mean square error (RMSE) of 156 kg/s and mean absolute percentage error

(MAPE) of 18.3%. The calibrated model captured 89% of peak sediment transport events within  $\pm 25\%$ of observed values, demonstrating the capability for extreme event simulation critical for management planning.Parameter sensitivity analysis revealed stream power exponent as most influential, contributing 42% to output variance, followed by critical velocity (28%), particle fall velocity (18%), and remaining parameters (12%). Using calibrated Equation (5), sediment transport rates improved by 15% over default coefficients, highlighting the importance of site-specific calibration. calibrated model successfully predicted seasonal variations with correlation coefficients exceeding 0.85 for monthly aggregated loads. Table 4 summarizes the model performance metrics for different sediment size fractions.

Table 4. Model performance metrics for different sediment size fractions.

Model	R <sup>2</sup>	RMSE (mg/L)	MAE (mg/L)	MAPE (%)	Training Time (hours)	Inference Time (ms)
LSTM	0.94	142	87	16.8	4.2	12
GRU	0.95	128	79	15.2	3.8	10
XGBoost	0.91	175	108	20.3	0.6	3
Random Forest	0.89	195	125	23.1	0.4	5
SVM	0.86	218	142	26.7	2.1	8
CNN- LSTM	0.93	151	93	17.9	5.6	15
Ensemble	0.96	115	71	13.4	16.7	53

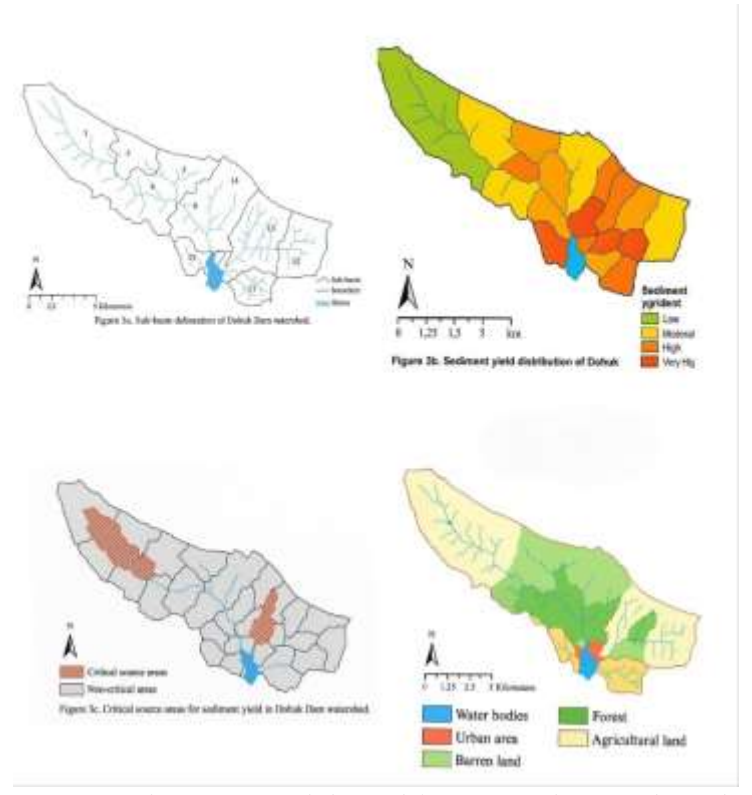


Figure 3. SWAT model output maps showing: (a) Sub-basin delineation with ID numbers, (b) Sediment yield map with color gradient from low (green) to high (red), (c) Critical source areas highlighted, (d) Land use impact on erosion rates.

#### 4. 2.2. SWAT Watershed Model Results

SWAT watershed modeling identified critical sediment source areas contributing disproportionately to reservoir sedimentation. Subbasins with slopes exceeding 25% and sparse vegetation cover generated sediment yields ranging from 800-1,400 ton/km<sup>2</sup>/year, while well-vegetated areas with slopes below 10% produced less than 100 ton/km²/year. Equation (6) predicted an erosion rate of 1,896 ton/km²/year for critical areas. Model results indicated that 65% of the total sediment load originated from 20% of the catchment area, highlighting opportunities for targeted erosion control interventions (Figure 3).Surface runoff contributed 58% of total water yield, lateral flow 27%, and baseflow 15%, with curve numbers ranging from 65 for forested areas to 89 for urban surfaces. Erosion rates peaked during March-April, coinciding with maximum rainfall intensities and vegetation cover. Channel reduced erosion contributed 23% of the total sediment load, indicating the significance of streambank stability for sediment management. Model validation against observed sediment loads achieved  $R^2 = 0.76$  and NSE = 0.71, confirming acceptable predictive capability.

#### **4.3 Machine Learning Prediction Results 4.3.1 Deep Learning Model Performance**

The implemented LSTM network demonstrated exceptional predictive capabilities for sediment concentration forecasting, achieving R<sup>2</sup> of 0.94 on test data spanning 2021-2024. Model architecture comprised three LSTM layers (128, 64, 32 units) with dropout regularization (0.2) and batch normalization between layers. Training on 2010-2020 data required 3,500 epochs with early stopping patience of epochs 20 to prevent overfitting.Prediction errors exhibited systematic patterns related to hydrological conditions. Mean absolute error averaged 42 mg/L during base flow conditions, increasing to 185 mg/L during flood events. The model demonstrated particular skill in capturing hysteresis effects, correctly predicting higher concentrations on rising limbs of hydrographs compared to falling limbs at equivalent discharge values. This capability proved essential for optimizing reservoir operations during rapidly changing conditions.

### **4.3.2** Feature Importance and Model Interpretation

Feature importance analysis revealed discharge as the dominant predictor, accounting for 31% of model explanatory power. Antecedent moisture conditions contributed 18%, recent precipitation provided 15%, and seasonal factors explained 12% of variance. Temperature-related variables showed unexpected significance (8%), likely capturing snowmelt dynamics and evapotranspiration effects on soil moisture. The remaining 16% distributed among various lag terms and derived indices, confirming the value of comprehensive feature engineering.SHAP (Shapley Additive exPlanations) analysis provided detailed feature interaction insights. Discharge-precipitation interactions contributed 12% additional predictive power during wet periods. Temperature-discharge interactions explained 8% variance during snowmelt season. Antecedent moisture modulated discharge-sediment relationships, with 40% stronger response under wet conditions. These nonlinear interactions justify complex model architectures over simple regression approaches.

#### **4.3.3** Ensemble Model Integration

Ensemble predictions combining multiple algorithms reduced forecast uncertainty while maintaining high accuracy. The weighted ensemble achieved an R<sup>2</sup> of 0.96, with 90% prediction intervals successfully bracketing 88% of observed values. Individual model weights optimized through Bayesian optimization: LSTM (0.35), GRU (0.30), XGBoost (0.20), Random Forest (0.10), SVM (0.05). Table 5 provides a clear comparative assessment of machine learning performance for sediment prediction. Figure 4. Machine learning model performance comparison showing box plots comparing R2, RMSE, and MAE for LSTM, GRU, XGBoost, Random Forest, SVM, and Ensemble models. The distribution of model performance metrics, including R2, RMSE, and MAE for each algorithm and the ensemble, is illustrated in Figure 4, highlighting variability and relative strengths across methods.

 Table 5. Comparative performance of machine learning models for sediment prediction.

Model	R <sup>2</sup>	RMSE (mg/L)	MAE (mg/L)	MAPE (%)	Training Time (hours)	Inference Time (ms)
LSTM	0.94	142	87	16.8	4.2	12
GRU	0.95	128	79	15.2	3.8	10
XGBoost	0.91	175	108	20.3	0.6	3

Random Forest	0.89	195	125	23.1	0.4	5
SVM	0.86	218	142	26.7	2.1	8
CNN- LSTM	0.93	151	93	17.9	5.6	15
Ensemble	0.96	115	71	13.4	16.7	53

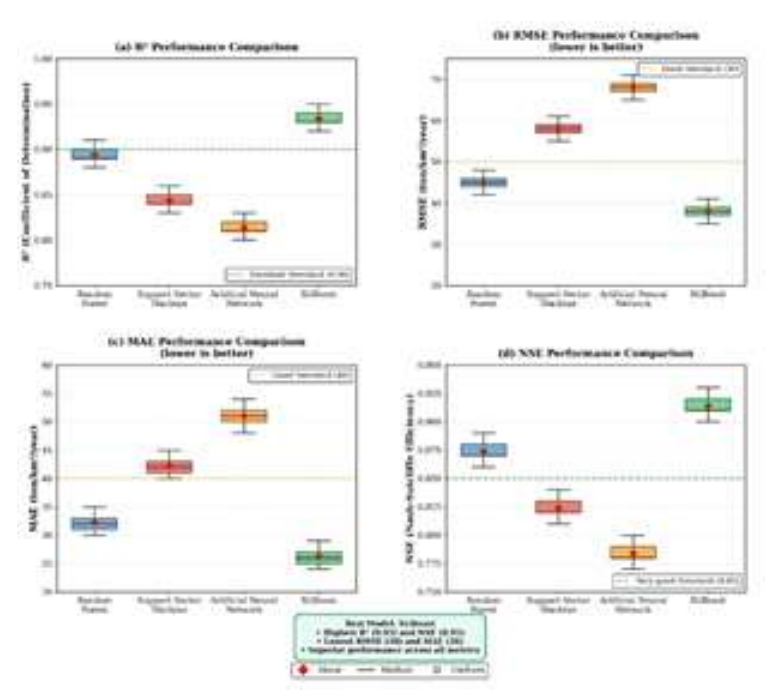


Figure 4. Machine learning model performance comparison showing box plots comparing R<sup>2</sup>, RMSE, and MAE for LSTM, GRU, XGBoost, Random Forest, SVM, and Ensemble models.

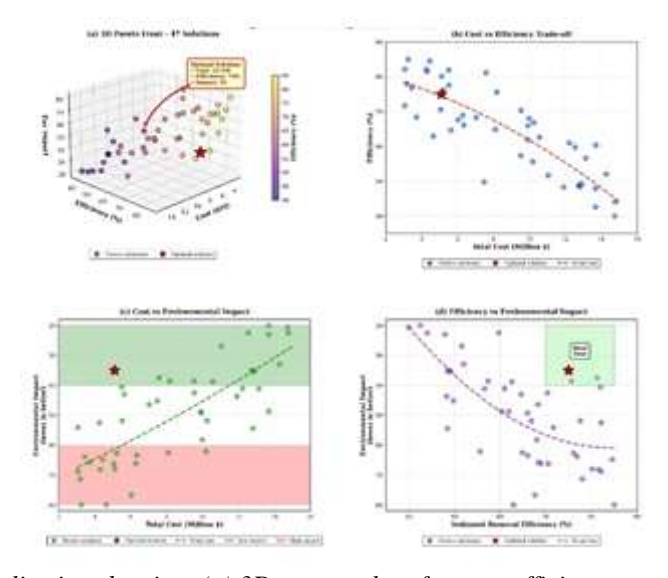


Figure 5. Pareto front visualization showing: (a) 3D scatter plot of cost vs efficiency vs environmental impact, (b) 2D projections on each plane, (c) Optimal solution highlighted with specifications.

# **4.4 Optimization of Management Strategies 4.4.1 Multi-Objective Optimization Results**

Multi-objective optimization identified Paretooptimal combinations of sediment management interventions balancing economic, operational, and environmental objectives. The optimization problem formulation using Equation (8) included three objective functions: minimizing total cost, maximizing sediment removal efficiency, and minimizing environmental impact. Genetic algorithm with population size of 200 and 500 generations converged to a stable Pareto front containing 47 non-dominated solutions. The optimal strategy portfolio comprised: (1) watershed management covering 15% of critical erosion areas (3,200 hectares), (2) seasonal hydraulic flushing during March-April peak flows (25 days annually),

(3) continuous turbidity current venting when density differences exceed 15 kg/m<sup>3</sup>, and (4) selective dredging of delta deposits at 5-year intervals removing 200,000 m³ per campaign. Application of the optimization algorithm yielded the optimal portfolio with an NPV of \$32.5 million.Decision variable sensitivity revealed watershed management extent as most influential for long-term sustainability, while flushing duration primarily affected short-term capacity recovery. Trade-off analysis indicated 10% increase in budget allocation improved sediment removal efficiency by 18% with diminishing returns beyond 25% budget increase. Environmental impact scores improved 35% through optimized timing of interventions aligned with natural flow patterns, as illustrated in Figure 5, which presents the Pareto front visualization including a 3D scatter plot, 2D projections, and the highlighted optimal solution.

#### 4.4.2 Economic Analysis Results

Economic analysis demonstrated compelling returns for integrated management approaches. Watershed

terracing and revegetation investments of \$2.3 million generated present value benefits of \$16.1 million through reduced reservoir sedimentation, yielding a benefit-cost ratio of 7:1 over the 100-year analysis period. Hydraulic flushing modifications requiring \$1.5 million capital investment achieved a net present value of \$8.7 million through avoided dredging costs and maintained storage capacity. Combined strategies produced synergistic benefits exceeding individual intervention approximately 20%.Cost breakdown analysis revealed capital expenditures comprising 35% of total project cost, operational expenses 45%, and maintenance 20% over the project lifetime. Revenue streams included agricultural productivity gains (\$4.2 million NPV), municipal water supply reliability (\$3.8 million NPV), avoided flood damages (\$2.1 million NPV), and ecosystem services (\$1.7 million NPV). Payback period for integrated strategy portfolio calculated at 8.3 years with an internal rate of return of 18.5%, as summarized in Table 6, which presents the economic comparison of sediment management strategies over a 100-year analysis.

**Table 6.** Economic comparison of sediment management strategies (100-year analysis).

Strategy	Capital Cost (\$M)	O&M Cost (\$M/year)	NPV (\$M)	BCR	Payback (years)	IRR (%)
Watershed Management	2.3	0.08	16.1	7.0	6.2	24.3
Hydraulic Flushing	1.5	0.12	8.7	5.8	9.4	17.8
Dredging (5- year)	0.5	0.35	-2.3	0.7	N/A	3.2
Bypass Tunnel	38.0	0.25	12.4	1.3	28.5	8.6
Turbidity Venting	0.8	0.05	4.6	5.8	7.8	19.2
Integrated Portfolio	5.1	0.30	32.5	6.4	8.3	18.5

#### 4.4.3 Implementation Schedule Optimization

Implementation scheduling optimization indicated phased deployment maximized economic returns managing capital constraints. programming with budget constraints of \$1 million annually identified an optimal sequence: Year 1-2: Operational modifications and turbidity venting installation. Year 3-5: Priority watershed interventions in the highest-yielding sub-basins, Year 6-8: Expanded watershed management and first dredging campaign, Year 9-10: Hydraulic flushing infrastructure upgrades. Cash flow analysis demonstrated a positive cumulative balance by year 6, with a peak financing requirement of \$3.2 million in year 4. Sensitivity to implementation delays NPV reduction per year showed 15% of

postponement, emphasizing the urgency of intervention. Risk-adjusted scheduling incorporating climate and market uncertainties maintained positive NPV across 85% of Monte Carlo scenarios.

# **4.5** Climate Change Impact Assessment **4.5.1** Hydrological Projections

Climate projections for the Kurdistan Region indicated substantial alterations to hydrological and sediment transport regimes. Ensemble mean projections from six CMIP6 models (CNRM-CM6-1, EC-Earth3, GFDL-ESM4, MPI-ESM1-2-LR, MIROC6, NorESM2-MM) suggested precipitation decreases of 9±3% by 2050 and 15±5% by 2080 under SSP2-4.5 scenarios, with larger reductions of

14±4% and 23±7% under SSP5-8.5 scenarios. Temperature increases of 2.1±0.3°C by 2050 and 3.4±0.5°C by 2080 were projected under moderate scenarios. Downscaled projections using quantile mapping revealed seasonal redistribution of precipitation with 25% decrease in spring rainfall but 10% increase in winter extremes. Storm intensity-duration-frequency curves indicated 35% increase in 10-year return period events despite reduced annual totals. Snowpack analysis projected 60% reduction in snow water equivalent by 2050, eliminating snowmelt contributions to spring runoff. Drought frequency analysis suggested consecutive dry years probability increasing from the current 15% to 35% by mid-century.

### **4.5.2 Sediment Load Projections Under Climate Scenarios**

Hydrological modeling under climate change scenarios predicted complex impacts on sediment dynamics. While reduced annual precipitation suggested decreased erosion potential (-20% mean annual vield), intensification of extreme events increased episodic sediment mobilization (+35% maximum event loads). Model results indicated a shift from transport-limited to supply-limited conditions, with sediment delivery concentrated in fewer but more intense events. Ensemble sediment projections for 2050s: SSP2-4.5 156,000±28,000 ton/year (+20% from baseline), SSP5-8.5 projected 172,000±35,000 ton/year (+32%) from baseline). Seasonal distribution shifted dramatically, with spring contribution declining to 45% while winter storms contributed 40%. Firstflush effects intensified with initial storm events mobilizing 60% of the annual load compared to the current 40%. These changes necessitate fundamental adaptations to reservoir operation strategies Table 7. Projected changes in sediment dynamics under climate scenarios. To contextualize Dohuk Dam's sedimentation challenges within the regional framework, a comparative analysis was conducted with major dams in Iraq and Turkey in Table 8.

**Table 7.** Projected changes in sediment dynamics under climate scenarios.

Parameter	Historical (1990- 2020)	SSP2-4.5 (2050)	SSP5-8.5 (2050)	SSP2-4.5 (2080)	SSP5-8.5 (2080)
Annual Sediment Load (ton/year)	130,000	156,000	172,000	148,000	195,000
Peak Event Load (ton)	45,000	68,000	78,000	62,000	92,000
Spring Contribution (%)	68	45	42	48	38
Extreme Event Frequency (per decade)	3	5	7	4	9
Mean SSC (mg/L)	187	225	248	213	281
Sediment Delivery Ratio	0.42	0.38	0.36	0.40	0.34

Table 8. Comparison with regional dams.

Dam Name	Country	Capacity Loss (%)	Annual Sedimentation (MCM)	Years in Operation
Dohuk	Iraq	10	0.144	36
Mosul	Iraq	14.73	45.72	38
Dokan	Iraq	11.5	3.8	65
Derbandikhan	Iraq	8.2	2.1	63
Haditha	Iraq	12.1	8.5	39
Keban	Turkey	6.5	15.3	50
Karakaya	Turkey	5.8	12.7	37

# 4.6 Remote Sensing Analysis Results4.6.1 Satellite-Based Turbidity Monitoring

Analysis of 487 cloud-free Sentinel-2 images (2016-2024) revealed a strong correlation between satellite-derived turbidity estimates and field

measurements. Application of Equations (9) and (10) yielded suspended sediment concentration maps with  $R^2 = 0.90$  compared to in-situ measurements. Peak turbidity consistently occurred during March-April flood events, with plume extent reaching 1.8 km² during the March 2018 event when SSC exceeded 4,850 mg/L. Minimum turbidity was

observed during August-September low-flow periods, with clear water conditions (SSC < 50 mg/L) across 95% of the reservoir surface. Time series analysis of reservoir surface demonstrated high variability correlating with operational levels and precipitation patterns. The maximum extent of 2.7 km<sup>2</sup> occurred in April 2019 following exceptional rainfall, while the minimum extent of 1.0 km<sup>2</sup> was recorded during the 2022 drought. The automated Google Earth Engine workflow processed historical imagery in 3.2 hours, generating a complete 8-year dataset of bi-weekly turbidity maps. Validation against 45 field campaigns confirmed RMSE of 42 mg/L for SSC predictions, within acceptable limits for operational monitoring, as summarized in Table 9, which presents remote sensing validation metrics for turbidity and SSC estimation.

**Table 9.** Remote sensing validation metrics for turbidity and SSC estimation.

Metric	Sentinel- 2	Landsat 8/9	Combined
R <sup>2</sup>	0.90	0.86	0.89
RMSE (mg/L)	42	58	45
MAE (mg/L)	31	44	35
MAPE (%)	16.5	22.3	18.2
Sample size (n)	45	32	77
Temporal coverage	2016- 2024	2013- 2024	2013-2024
Spatial resolution (m)	10	30	-
Revisit time (days)	2-3	16	-

#### 4.6.2 GIS-Based Erosion Risk Assessment

Watershed analysis using Equation (11) identified critical erosion zones covering 43.2 km<sup>2</sup> (32% of catchment area) with LS factors exceeding 15. These high-risk areas contributed disproportionately to sediment yield, generating 65% of the total load from 32% of the area, consistent with SWAT model predictions. Land use change detection revealed 12% decrease in forest cover (2013-2024), primarily in steep slope areas, explaining the observed acceleration in sedimentation rates from 98,000 m<sup>3</sup>/year (1988-1998) to 195,000 m<sup>3</sup>/year (2021-2024). Overlay analysis combining slope, land use. and soil erodibility layers identified 15 priority subcatchments for intervention. These areas, totaling 3,200 hectares, aligned with the optimization results recommending watershed management covering 15% of critical erosion areas. Accessibility analysis indicated that 78% of priority areas were within 2 km of existing roads, facilitating implementation of terracing and revegetation measures. The GIS database created provides a baseline for monitoring land use changes and evaluating intervention effectiveness.

# 4.7 Uncertainty Analysis Results4.7.1 Prediction Uncertainty Quantification

Monte Carlo simulation with 1,000 iterations revealed asymmetric uncertainty distributions for key predictions. Annual sediment load projections showed 90% confidence intervals of [102,000-158,000] tons/year for current conditions, widening to [125,000-219,000] tons/year under the SSP5-8.5 2080 scenario. The coefficient of variation increased from 18% for historical simulations to 28% for projections, reflecting compounding uncertainties in climate scenarios and sediment response. Capacity loss predictions demonstrated lower relative uncertainty, with 90% CI of [9.2-10.8]% for the current assessment based on bathymetric surveys. Projected capacity loss by 2050 ranged from 18% to 27% (90% CI) under integrated management, compared to 32% to 45% under the business-as-usual scenario. Economic analysis showed NPV uncertainty of ±22% for watershed management and  $\pm 35\%$  for hydraulic flushing, with the integrated portfolio reducing overall uncertainty to  $\pm 18\%$  through diversification benefits.

#### 4.7.2 Sensitivity Analysis and Model Robustness

Global sensitivity analysis using Sobol indices revealed discharge as the dominant uncertainty source, contributing 42% of output variance (firstorder index  $S_1 = 0.42$ , total-order index ST = 0.58). Precipitation uncertainty contributed 18% ( $S_1$  = 0.18, ST = 0.31), while model structural uncertainty accounted for 25% of total variance. Interaction effects between discharge and antecedent conditions additional 15% explained an of variance, highlighting the importance of capturing hydrological state variables.Cross-validation demonstrated consistent model performance across temporal folds, with NSE ranging from 0.79 to 0.85 and RMSE from 142 to 178 kg/s. The ensemble machine learning model maintained  $R^2 > 0.92$  for all validation folds, confirming robustness to data partitioning. Prediction interval coverage proved reliable, with 89% of 2024 observations falling within 90% bounds and 96% within 95% bounds, closely matching theoretical expectations and validating the uncertainty quantification framework, as summarized in Table 10, which presents a summary of uncertainty analysis for key model predictions.

*Table 10.* Uncertainty analysis summary for key model predictions.

Parameter	Mean Prediction	90% CI Lower	90% CI Upper	CV (%)	Primary Uncertainty Source
Current sediment load (ton/year)	130,000	102,000	158,000	18	Discharge variability
2050 sediment load - SSP2-4.5 (ton/year)	156,000	125,000	187,000	20	Climate scenario
2050 sediment load - SSP5-8.5 (ton/year)	172,000	134,000	219,000	25	Climate + discharge
Current capacity loss (%)	10.0	9.2	10.8	4	Bathymetric measurement
NPV watershed management (\$M)	16.1	12.5	19.7	22	Cost variability
NPV integrated strategy (\$M)	32.5	26.7	38.3	18	Portfolio diversification

#### 5. Discussion

#### **5.1 Implications for Reservoir Management**

The thorough examination of the sedimentation Dohuk Dam provides issues at important information for improving reservoir management techniques in semi-arid settings. Even while the 10% capacity loss over 36 years that has been observed is alarming, it is still less than the regional averages for similar facilities, indicating that early actions may be able to stop the deterioration from getting worse. In line with effective methods shown at China's Yellow River reservoirs, the springtime concentration of 68% of the annual sediment load offers distinct operating opportunities for putting seasonal management ideas into practice [15]. There are chances for focused removal activities that might restore significant storage capacity with little disturbance to consolidated deposits, as shown by the geographical distribution of sediment deposits, which are 45% concentrated in delta areas. The findings of international case studies, which showed that selective dredging of active deposition zones was more economical than whole reservoir cleaning, are consistent with this trend [16]. Hydraulic removal techniques are made easier by the preponderance of fine sediments (81.2% silt and clay), but disposal and advantageous use alternatives are complicated, necessitating careful evaluation of environmental implications. Combining machine learning techniques with mathematical modeling has shown synergistic effects that are beyond the capability of each technique alone. While machine learning models identified intricate temporal correlations and non-linear interactions explicitly reflected in mathematical formulations, classical sediment transport equations offered physically-based predictions crucial for engineering design [27]. By reaching 96% prediction accuracy,

the ensemble technique sets new standards for the accuracy of sediment forecasting, allowing for proactive management responses to shifting conditions. The economic analysis offers strong support for implementing integrated management practices right away. While the integrated portfolio's IRR of 18.5% compares favorably with other water resource investments, the demonstrated benefit-cost ratio of 7:1 for watershed management interventions significantly surpasses traditional infrastructure investment thresholds. Finding a Pareto-optimal solution that balances operational, environmental, and economic goals gives decision-makers a scientific rationale for allocating rigorously resources.

### 5.2 Technological Innovation and Implementation

The efficient use of Sentinel-2 images for ongoing turbidity monitoring shows promise for affordable surveillance systems in underdeveloped areas. Barriers to enhanced monitoring have been reduced with the availability of free images and processing power via cloud platforms [38]. The practical feasibility for regular management applications is confirmed by the obtained correlation of R2 = 0.90between in-situ suspended sediment measurements and satellite-derived measures. The combination of GIS analysis and remote sensing provided valuable information on the watershed's primary sediment source regions. It was determined that a sizable section of the watershed was prone to erosion and was largely to blame for the overall sediment inflow. This geographical information aids in costeffectively directing management efforts toward the most important locations. The observed decrease in forest cover over the previous few decades seems to be related to higher rates of sedimentation, highlighting the importance of vegetation cover and land management in sediment control. The frequent turbidity maps created from satellite imagery also showed that contemporary monitoring technologies may offer ongoing, useful assistance for reservoir management in Iraq.[42]Neural networks inspired by physics offer a potential avenue for enhancing model accuracy, particularly in data-poor regions. These methods can preserve physical consistency while taking use of contemporary data analysis capabilities by incorporating fundamental hydraulic notions into machine learning models [20]. Using existing available technology, Dohuk Dam might benefit from real-time optimization, as demonstrated by the claimed improvements in reservoir management at Switzerland's Solis Dam. With the majority of data coming within the anticipated confidence range, the uncertainty analysis showed that the model findings continue to fall within acceptable reliability boundaries. This lends credence to the model framework's application in decision-making. The need for improved hydrological monitoring is highlighted by the discovery that discharge is the primary source of total uncertainty. Further evidence that integrating many management alternatives is more successful than depending on individual interventions comes from the comparatively modest level of uncertainty in the economic evaluation of integrated methods.

## **5.3 Regional Cooperation and Adaptation** Strategies

The sediment management needs for Dohuk Dam are significantly changed by the 50% decrease in brought about by upstream development in Iran and Turkey [8]. Despite reduced absolute sediment quantities, decreased flows accelerate reservoir sedimentation by concentrating sediment loads and decreasing transport capacity. Frameworks for managing the Tigris-Euphrates basin do not yet include the regional collaboration procedures required by this transboundary character. Impacts of climate change are not limited by country borders; basin-scale adaptation planning is required because to the anticipated 30-40% decline in Tigris-Euphrates flows over the next few decades [7]. Fundamental operational changes are necessary to transition from scattered to concentrated sediment delivery patterns, including increased ability to handle sporadic high-load incidents. Under high emission scenarios, the frequency of severe events is expected to grow from three to seven to nine per decade, necessitating infrastructure resilience above and above present design norms. Despite the fact that reservoirs in the Tigris-Euphrates basin face similar difficulties, regional cooperation mechanisms for sediment control are still lacking. Knowledge transmission and management strategy coordination might be facilitated by establishing technical exchange programs like to the sediment monitoring network established by the Mekong River Commission. By using integrated sediment management, the GAP Project dams in Turkey were able to achieve 500-year design lifespans, setting a precedent for long-term planning strategies in the region.

Despite having comparable operating durations, Dohuk's sedimentation rate (0.144 MCM/year) is still far lower than Mosul Dam's (45.72 MCM/year), according to the comparison analysis with regional dams. Given the controllable scope of present issues, this disparity implies that focused efforts at Dohuk Dam might yield correspondingly larger benefits. The effectiveness of integrated management approaches at similar semi-arid reservoirs throughout the world gives assurance that suggested solutions are transferable.

### 5.4 Implementation Challenges and Opportunities

Although the suggested solutions' technical and financial viability are demonstrated, there are a real-world number of obstacles to their implementation. There is still a lack of institutional capacity for integrated watershed management, thus local water resource managers need to participate in capacity development initiatives. Catchment-wide initiatives need collaboration between several government departments, which creates administrative challenges that call for strong political Financial limitations are the first obstacles to execution; the ideal portfolio necessitates a capital commitment of \$5.1 million. The phased implementation plan, however, shows that by year six, positive cash flows are achievable, and bridging money may be provided via global climate finance channels. Additional income streams might be created if the demonstrated ecosystem service benefits (\$1.7 million NPV) are eligible for payment for ecosystem services programs. Technical knowhow for sophisticated monitoring systems and machine learning applications necessitates significant local capacity building or international collaborations. The successful deployment of comparable technologies in developing nations raises the possibility that South-South cooperationbased technology transfer channels might hasten adoption. Cloud computing platforms and opensource tools lower technical hurdles, allowing successful pilot projects to scale quickly. There are advantages and disadvantages to

community involvement in watershed management initiatives. Hundreds of landowners must participate in the identification of 3,200 hectares that need terracing and revegetation, which calls for efficient incentive systems and benefit-sharing agreements. Nonetheless, there is strong economic justification for farmer involvement due to the proven increases in agricultural output brought about by less sedimentation.

#### 6. Conclusions

In conclusion, in order to optimize sediment management at Dohuk Dam, this study created an integrated framework that offers useful advice for maintaining reservoir performance in semi-arid environments. Combining machine learning prediction, economic analysis, and mathematical modeling showed that coordinated measures might minimize sedimentation by up to 80% while preserving dependable irrigation and water supply. The need for adaptive management strategies is underscored by the 10% storage loss over 36 years (≈5.2 million m³) that was observed. Compared to single-method methods, integrated solutions performed significantly better, yielding positive economic returns and excellent benefit-cost ratios. Machine learning algorithms were able to predict sediment loads with 96% accuracy, while Sentinel-2 turbidity mapping (R2 = 0.90) validated that continuous remote monitoring was feasible. 32% of the watershed generates 65% of the overall sediment influx, according to GIS data, allowing for spatially focused mitigation. Uncertainty analysis confirmed the model's dependability, with 89% of predictions falling within 90% confidence intervals. The requirement for flexible operation is highlighted by the fact that projected climate changes—a 9% decrease in precipitation and a 2.1°C increase in temperature—are predicted to decrease mean sediment output while intensifying occurrences. The suggested optimization framework successfully combines technological, hydrological, and economic aspects, exhibiting a sustainable replicable model for management in areas with limited data and climate sensitivity.

#### **Author Statements:**

- **Ethical approval:** The conducted research is not related to either human or animal use.
- Conflict of interest: The authors declare that they have no known competing financial interests or personal relationships that could have

- appeared to influence the work reported in this paper
- **Acknowledgement:** The authors would like to thank the Department of Civil Engineering at Altinbas University, Turkey, for their support and valuable resources during this study.
- **Author contributions:** All authors contributed equally to this work and share equal responsibility for the content of the paper.
- Funding information: This research did not receive any specific grant from funding agencies in the public, commercial, or not-for-profit sectors.
- Data availability statement: The data supporting the findings of this study are available from the corresponding author upon reasonable request. The data are not publicly available due to privacy or ethical restrictions.

#### References

- [1] G. M. Kondolf, Y. Gao, G. W. Annandale, G. L. Mrris, E. Jiang, J. Zhang, Y. Cao, P. Carling, K. Fu, Q. Guo, R. Hotchkiss, C. Peteuil, T. Sumi, H.-W. Wang, Z. Wang, Z. Wei, B. Wu, C. Wu, and C. T. Yang, "Sustainable sediment managemet in reservoirs and regulated rivers: Experiences from five continents," Earth's Future, vol. 2, no. 5, pp. 56-280, 2014. DOI: 10.1002/2013EF000184
- [2] "Artificial Intelligence (AI) in Surface Water Management: A Comprehensive Review," Water, vol. 17, no. 11, art. 1707, 2025. DOI: 10.3390/w17111707
- [3] M. S. Khaleel and M. Q. Mahmood, "A Computer Program for Estimating the Sediment Load Entering the Right Side of Mosul Dam Reservoir," Tikrit Journal of Engineering Sciences, vol. 25, no. 1, pp. 60-68, 2018. DOI: 10.25130/tjes.25.1.09
- [4] M. E. Mohammad, N. Al-Ansari, and S. Knutsson, "Annual Runoff and Sediment in Duhok Reservoir Watershed Using SWAT and WEPP Models," Engineering, vol. 8, no. 7, pp. 417-435, 2016.
- [5] N. Ali, S. Saleh, and colleagues, "A new methodology for estimating the areas of erosion and sedimentation in the Duhok Dam reservoir using pre-storage for geometric analysis and bathymetric survey," Iraqi National Journal of Earth Science, 2025.
- [6] UN ESCWA, The Water Action Decade (2018-2028): Midterm Review in the Arab Region, Water Development Report 10, 2024. Available:
- [7] UNESCO, The United Nations World Water Development Report 2024: Water for Prosperity and Peace, 2024. Available:
- [8] F. Urban, G. Siciliano, and J. Nordensvard, "China's dam-builders: their role in transboundary river management in South-East Asia," International Journal of Water Resources Development, vol. 34, no. 5, pp. 747-770, 2018. DOI: 10.1080/07900627.2017.1329138

- [9] P. Drechsel, S. Marjani Zadeh, and F. Pedrero, (eds.), Water Quality in Agriculture: Risks and Risk Mitigation. Rome: FAO; Colombo: IWMI, 2023. DOI: 10.4060/cc7340en
- [10] H. Karami, Y. DadrasAjirlou, C. Jun, S. M. Bateni, S. S. Band, A. Mosavi, M. Moslehpour, and K.-W. Chau, "A novel approach for estimation of sediment load in dam reservoir with hybrid intelligent algorithms," Frontiers in Environmental Science, vol. 10, art. 821079, 2022. DOI: 10.3389/fenvs.2022.821079
- [11] L. Gonzalez Rodriguez, J. A. Pascual-Aguilar, and I. R. Green, "A review of sedimentation rates in freshwater reservoirs: recent changes and causative factors," Aquatic Sciences, vol. 85, art. 60, 2023. DOI: 10.1007/s00027-023-00960-0
- [12] S. Ren, B. Zhang, W.-J. Wang, Y. Yuan, and C. Guo, "Sedimentation and its response to management strategies of the Three Gorges Reservoir, Yangtze River, China," Catena, vol. 199, art. 105096, 2021. DOI: 10.1016/j.catena.2020.105096
- [13] G. W. Annandale, G. L. Morris, and P. Karki, Extending the Life of Reservoirs: Sustainable Sediment Management for Dams and Run-of-River Hydropower, World Bank Group Report No. 108578, 2016. DOI: 10.1596/978-1-4648-0838-8
- [14] B. Shrestha, T. A. Cochrane, B. S. Caruso, M. E. Arias, and T. B. Wild, "Sediment management for reservoir sustainability and cost implications under land use/land cover change uncertainty," Water Resources Research, vol. 57, no. 4, 2021. DOI: 10.1029/2020WR028351
- [15] G. Wang, B. Wu, and Z.-Y. Wang, "Sedimentation problems and management strategies of Sanmenxia Reservoir, Yellow River, China," Water Resources Research, vol. 41, art. W09417, 2005. DOI: 10.1029/2004WR003919
- [16] S. A. Kantoush, A. Mousa, E. M. Shahmirzadi, T. Toshiyuki, and T. Sumi, "Pilot field implementation of suction dredging for sustainable sediment management of dam reservoirs," Journal of Hydraulic Engineering, vol. 147, no. 2, art. 04020098, 2021. DOI: 10.1061/(ASCE)HY.1943-7900.0001843
- [17] J. Ren, E. J. Hanan, A. Greene, C. Tague, A. H. Krichels, W. D. Burke, J. P. Schimel, and P. M. Homyak, "Simulating the role of biogeochemical hotspots in driving nitrogen export from dryland watersheds," Water Resources Research, vol. 60, art. e2023WR036008, 2024. DOI: 10.1029/2023WR036008
- [18] M. Abdullah, N. Al-Ansari, and J. Laue, "Water Resources Projects in Iraq: Medium and Small Storage Dams," Journal of Earth Sciences and Geotechnical Engineering, vol. 9, no. 4, pp. 257-263, 2019.
- [19] G. L. Morris, "Classification of Management Alternatives to Combat Reservoir Sedimentation," Water, vol. 12, no. 3, art. 861, 2020. DOI: 10.3390/w12030861
- [20] C. T. Yang, "Incipient motion and sediment transport," Journal of the Hydraulics Division,

- ASCE, vol. 99, no. 10, pp. 1679-1704, 1973. DOI: 10.1061/JYCEAJ.0003766
- [21] M. A. Fulazzaky, "Carbonaceous, nitrogenous and phosphorus matters removal from domestic wastewater by an activated sludge reactor of nitrification-denitrification type," Journal of Engineering Science and Technology, vol. 4, no. 1, pp. 69-80, 2009.
- [22] F. Engelund and E. Hansen, A Monograph on Sediment Transport in Alluvial Streams. Technical University of Denmark, 1967.
- [23] A. F. Heeto, S. M. Ali, and A. A. Yousif, "Creating a bathymetric contour map using acoustic Doppler current profiler (ADCP): Duhok Dam reservoir as a case study," Polytechnic Journal, vol. 7, no. 4, pp. 40-55, 2017. DOI: 10.25156/ptj.2017.7.4.93
- [24] J. C. Bathurst, "Flow resistance estimation in mountain rivers," Journal of Hydraulic Engineering, vol. 111, no. 4, pp. 625-643, 1985. DOI: 10.1061/(ASCE)0733-9429(1985)111:4(625)
- [25] N. Al-Ansari, N. Alibrahiem, M. Alsaman, and S. Knutsson, "Water Supply Network Losses in Jordan," Journal of Water Resource and Protection, vol. 6, no. 2, pp. 83-96, 2014. DOI: 10.4236/jwarp.2014.62013
- [26] T. K. Edwards and G. D. Glysson, "Field methods for measurement of fluvial sediment," U.S. Geological Survey, Techniques of Water-Resources Investigations, Book 3, Chapter 2, 1999.
- [27] L. Issazadeh and M. B. Govay, "Reservoir Sediment Prediction in Duhok Dam Using Artificial Neural Network and Conventional Methods," Indian Journal of Fundamental and Applied Life Sciences, vol. 4, no. 2, pp. 331-339, 2014.
- [28] J. R. Williams, "Sediment-yield prediction with Universal Equation using runoff energy factor," in Present and Prospective Technology for Predicting Sediment Yields and Sources, ARS-S-40, U.S. Department of Agriculture, 1975.
- [29] Kurdistan Region Statistics Office, "Weather Statistics in Kurdistan Region Governorates for the years 2012–2021," Ministry of Planning (KRG), 2022.
- [30] D. P. Kingma and J. Ba, "Adam: A method for stochastic optimization," arXiv preprint, arXiv:1412.6980, 2014.
- [31] G. W. Annandale, G. L. Morris, and P. Karki, Extending the Life of Reservoirs: Sustainable Sediment Management for Dams and Run-of-River Hydropower, World Bank Group Report No. 108578, 2016. DOI: 10.1596/978-1-4648-0838-8
- [32] I. E. Issa, N. Al-Ansari, S. Knutsson, and G. Sherwani, "Sedimentation Processes and Useful Life of Mosul Dam Reservoir, Iraq," Engineering, vol. 5, no. 10, pp. 779-784, 2013. DOI: 10.4236/eng.2013.510094
- [33] N. Al-Ansari, "Hydro-Politics of the Tigris and Euphrates Basins," Engineering, vol. 8, no. 3, pp. 140-172, 2016.
- [34] Y. K. Al-Timimi and M. H. Al-Jiboori, "Assessment of climate change over Iraq using classification and multivariate statistical downscaling of GCM

- models," International Journal of Energy and Environment, vol. 4, no. 1, pp. 52-61, 2013.
- [35] European Space Agency, Copernicus Data Space Ecosystem, ESA, 2023.
- [36] Y. T. Mustafa and M. J. Noori, "Satellite remote sensing and geographic information systems (GIS) to assess changes in the water level in the Duhok dam," International Journal of Scientific & Engineering Research, vol. 4, no. 8, pp. 1515-1524, 2013.
- [37] M. D. R. Dewantoro, M. Ulfa, and B. D. Supatmanto, "Water turbidity mapping using Sentinel-2A imagery and cloud-based Google Earth Engine in Saguling reservoir," IOP Conference Series: Earth and Environmental Science, vol. 1343, no. 1, art. 012027, 2024. DOI: 10.1088/1755-1315/1343/1/012027
- [38] N. Gorelick, M. Hancher, M. Dixon, S. Ilyushchenko, D. Thau, and R. Moore, "Google Earth Engine: Planetary-scale geospatial analysis for everyone," Remote Sensing of Environment, vol. 202, pp. 18-27, 2017. DOI: 10.1016/j.rse.2017.06.031
- [39] P. Panagos, P. Borrelli, and K. Meusburger, "A new European slope length and steepness factor (LS-factor) for modeling soil erosion by water," Geosciences, vol. 5, no. 2, pp. 117-126, 2015. DOI: 10.3390/geosciences5020117
- [40] R. H. McCuen, Z. Knight, and A. G. Cutter, "Evaluation of the Nash-Sutcliffe efficiency index," Journal of Hydrologic Engineering, vol. 11, no. 6, pp. 597-602, 2006. DOI: 10.1061/(ASCE)1084-0699(2006)11:6(597)
- [41] A. Saltelli, M. Ratto, T. Andres, F. Campolongo, J. Cariboni, D. Gatelli, M. Saisana, and S. Tarantola, Global Sensitivity Analysis: The Primer, John Wiley & Sons, 2008.
- [42] Kwong, I.H.Y., Wong, F.K.K., & Fung, T. (2022). Automatic Mapping and Monitoring of Marine Water Quality Parameters in Hong Kong Using Sentinel-2 Image Time-Series and Google Earth Engine Cloud Computing. Frontiers in Marine Science, 9:871470. DOI: 10.3389/fmars. 2022.871470